Available online at www.sciencedirect.com

Manufacturing Letters

Manufacturing Letters 44 (2025) 816–824

53rd SME North American Manufacturing Research Conference (NAMRC 53, 2025)

Additive manufacturing of radially oriented gyroid carbon fiber composites for low-temperature thermal absorber applications

Muhtadin Muhtadin[a], Semih Akin[b], Jung Ting-Tsai[a,*]

[a]*Department of Mechanical Engineering, National Taiwan University of Science and Technology, No. 43, Sec. 4, Keelung Rd., Taipei 106, Taiwan, ROC*
[b]*Department of Mechanical, Aerospace and Nuclear Engineering, Rensselaer Polytechnic Institute, Troy, NY 12180, USA*

* Corresponding author. Tel.: (02) 2737-6489; fax: +886-2-2737-6460. E-mail address: tsaij@mail.ntust.edu.tw

Abstract

This study evaluates the thermal-hydraulic performance of additively manufactured Radially Oriented Gyroid (RO-Gyroid) structures produced via Digital Light Processing (DLP) for applications in low-temperature thermal absorbers. Various gyroid configurations are designed and additively manufactured by considering key geometric parameters (viz., porosity, volume, surface area, specific surface area, hydraulic diameter). The effects of the geometric design parameters on heat transfer and pressure drop were studied to identify a dedicated gyroid structure that maximizes convective heat transfer while minimizing pressure drop. Experimental findings reveal that configurations with higher specific surface areas, like A9R6, achieved promising convective heat transfer 273.85 $Wm^{-2}.K^{-1}$ and a Performance Evaluation Criterion (PEC) of 5.89, balancing efficiency and pressure loss. On the one hand, high-porosity designs, such as A5R10, yielded a low pressure drop up to 50 Pa but exhibited reduced thermal performance due to limited surface area. Results suggest that increased arc count enhances heat transfer by up to 30%, whereas a larger cell radius reduces effective surface area, thereby impacting resulting heat transfer performance. Overall, an optimal gyroid design (A9R6) was identified for balancing heat transfer and pressure drop, offering valuable insights for low-temperature thermal absorber applications.

Peer-review under responsibility of the scientific committee of the NAMRI/SME.
Keywords: Additive manufacturing; gyroid structure; TPMS; thermal absorber; heat transfer; digital light processing

1. Introduction

Global energy consumption and the urgent demands for addressing climate change are driving encouraged investigation into clean and renewable energy [1,2]. Thermal systems are very efficient in such applications, including household water heating, space heating, and low-temperature industrial operations [3–5]. Traditionally, straight tubes coated with materials like black nickel and copper have been used to enhance heat transfer [6]. While these tubes offer advantages (e.g., ease of manufacturability, low cost), opportunities remain for further heat transfer improvement through geometrical design modifications. To this end, various innovative approaches have been proposed to enhance the absorber performance by leveraging unique geometries that promote heat transfer and induce turbulent flow [7]. These methods include designs featuring twisted tape shapes [8,9], wire coil shapes [7], toroidal rings[10], twisted strips with angular shapes [11] and baffles with curved and conical strips [12].

Most recently, gyroid structures have garnered substantial attention in the field of heat transfer due to their unique, complex geometry that provides an optimal balance of surface area and permeability [13]. The high-surface-area-to-volume ratio and lightweight design make gyroid structures ideal for high thermal performance with minimal material use [14]. In this context, Triply Periodic Minimal Surface (TPMS) structures are highly effective for heat transfer optimization due to their three-dimensional periodicity, which can be precisely designed through mathematical formulations. Their high surface area, lightweight properties, and mechanical strength

Peer-review under responsibility of the scientific committee of the NAMRI/SME.

make them ideal for thermal applications [15]. Benjamin W. et al. [16] characterized various TPMS types- such as gyroid, primitive, and diamond—for heat exchangers, finding that gyroid structures increased the Nusselt number (i.e., a dimensionless quantity that indicates the enhancement of convective heat transfer) by 13% over traditional straight-tube designs. While TMPS structures enhance heat transfer, some studies have shown that these structures often face issues related to undesired pressure drops, thereby necessitating a balance for optimal thermal-hydraulic performance [17–19]. As such, it is crucial to carefully design TPMS geometries using high-performance materials to maximize thermal performance while minimizing hydraulic resistance.

Over the last decade, additive manufacturing (AM) has found remarkable applications in the field of thermal absorber applications due to its ability to create intricate geometries from low-cost materials that enhance heat transfer efficiency and overall thermal performance [20,21]. AM techniques, including [16], Digital Light Processing (DLP) [22–29], laser powder bed fusion (LPBF) [30], fused deposition modelling (FDM) [31], directed energy deposition (DED) [20], were employed to fabricate TPMS structures, aiming to boost thermal performance. Collectively, these studies have laid the groundwork for AM-based thermal absorbers in practical applications [21,32]. Among these methods, DLP method stands out for its high precision and capability to produce complex lattice structures [22,23], which are ideal for optimizing surface area and fluid flow in thermal applications. DLP leverages ultraviolet light (UV) to selectively cure photopolymer resins layer by layer, enabling the production of intricate and highly detailed structures [22]. DLP offers significant advantages in designing and manufacturing complex structures such as gyroid structures, particularly through creating optimized lattice structures. Although several studies have utilized DLP technology in the fabrication of lattice structures for thermal applications, leading to substantial advancements [26–29], further exploration is needed to uncover the potential of DLP technology for lattice structures made of high-performance materials, aiming to enhance thermal and fluid dynamic performance.

Despite researchers have investigated TPMS structures, particularly gyroid structures, for thermal applications (e.g., heatsinks, heat exchangers, heat absorbers, reactors), significant gaps remain in optimizing thermal absorbers to enhance heat transfer while minimizing pressure drop. Furthermore, traditional designs have been widely studied but often fail to achieve the ideal balance between heat transfer and pressure drop. DLP 3D printing has shown potential for fabricating complex structures. However, limited research has focused on the fabrication of composite carbon fiber for specific applications, such as low-temperature thermal absorber.

This study focuses on the development of gyroid structures by leveraging the unique capabilities of the DLP-based AM. First, Radially Oriented Gyroid (RO-Gyroid) structures composed of composite carbon fiber was designed and fabricated via DLP, with careful consideration of various design configurations, including porosity, wall thickness, volume, surface aera, and hydraulic diameter. Subsequently, the thermal and hydraulic performance of the RO-Gyroid was experimentally characterized, focusing on optimizing arc count and cell radius to enhance heat transfer while minimizing the pressure drop. The main goals are to: (i) test DLP-based AM of gyroid structures comprising carbon fibers; (ii) assess 3D-printed composite structures for thermal absorbers; and (iii) optimize RO-Gyroid geometry for maximum thermal efficiency. Experimental results revealed critical insights into how structural and material design parameters (i.e., porosity, wall thickness, thermal conductivity) affect the overall heat transfer rate and fluid dynamics of the developed RO-Gyroid structure in thermal absorber applications.

Nomenclature

A	Arc account
A_G	Wetted surface area (mm^{-1})
A_h	Surface area (m^2)
A_{in}	Inlet cross-sectional area (m^2)
c	specific heat capacity of fluid ($J.kg^{-1}.K^{-1}$)
CAD	Computer-aided design
DED	Directed energy deposition
D_h	Hydraulic diameter (m)
f	Friction factor (-)
FDM	Fused deposition modelling
h	Convective heat transfer ($Wm^{-2}.K^{-1}$)
k	Thermal conductivity ($Wm^{-1}.K^{-1}$)
L	Length (m)
LPBF	Laser powder bed fusion
Nu	Nusselt number (-)
PEC	Performance Evaluation Criterion (-)
R	Cell radius (m)
r	RO-Gyroid radius (m)
Re	Reynold number (-)
SA	Surface area (mm^2)
T_A	Temperature heating surface (K)
T_{in}	Inlet temperature (K)
T_{out}	Outlet temperature (K)
U	Uncertainty (%)
v	Fluid velocity ($m.s^{-1}$)
θ	Arc angle (^{0})
λ	Thermal conductivity of the fluid ($W.m^{-1}.K^{-1}$)
Δp	Pressure drop (Pa)
ε	Porosity (-)
μ	Fluid dynamic viscosity ($kg.\ m^{-1}s^{-1}$)
P	Fluid density ($kg.m^{-3}$)

2. Materials and methods

This section details the design approach for generating radially oriented gyroid (RO-Gyroid) configurations, utilizing a mathematical framework [33,34]. The design configuration is expressed by the following implicit function.

$$\sin(x)\cos(y) + \sin(y)\cos(z) + \sin(z)\cos(x) = 0 \quad (1)$$

RO-Gyroid configurations were designed using nTop Platform (*nTopology software*). **Fig. 1(a)** illustrates the transformation of a conventional cubic gyroid into a radially

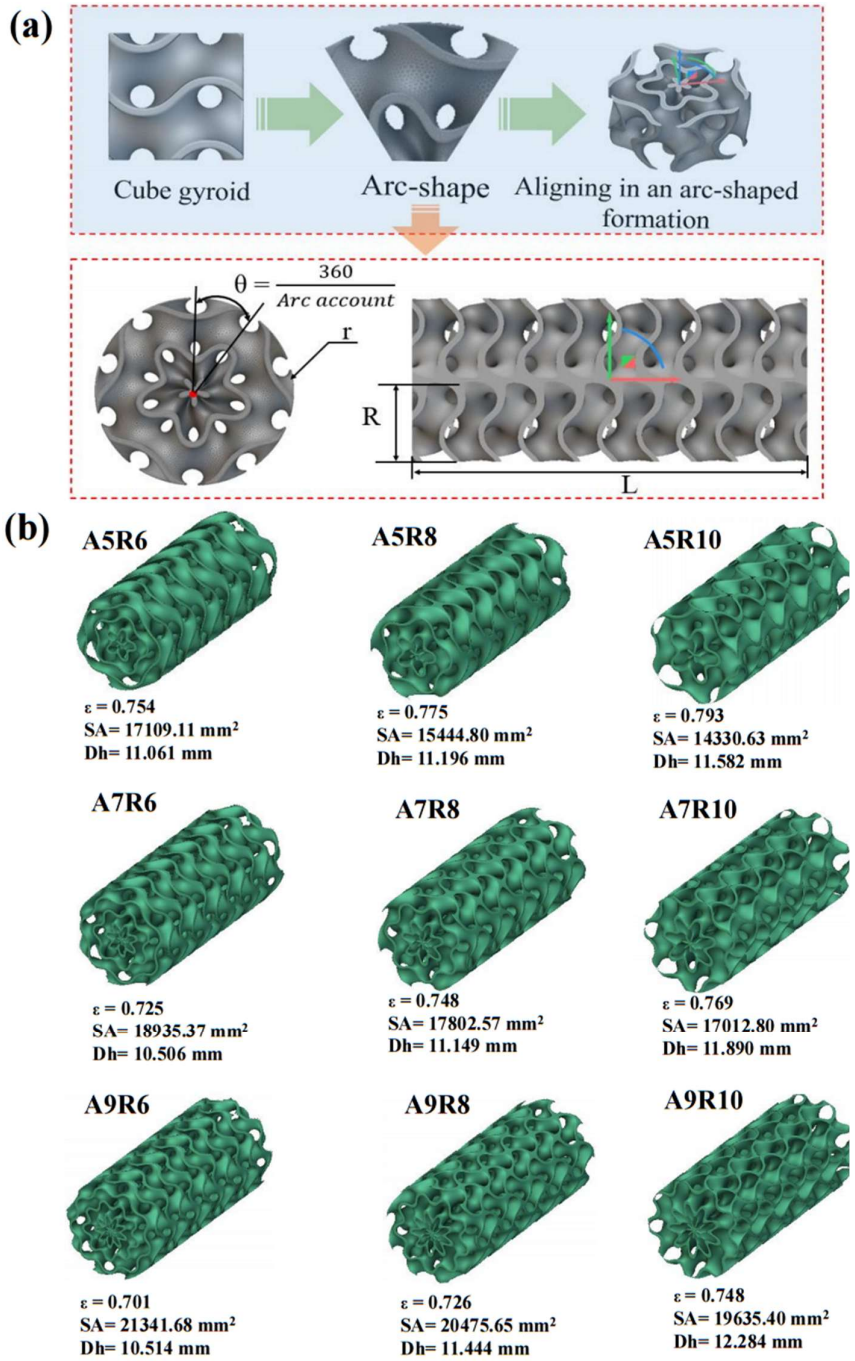

Fig. 1. (a) Transformation of a conventional gyroid to RO-Gyroid. **(b)** CAD of the various gyroid configurations considered in this work.

Table 1. Geometric characteristics of RO-Gyroid configurations with a 1 mm wall thickness

RO-Gyroid configuration	Porosity (ε)	Volume (mm^3)	Specific surface area (mm^{-1})
A5R6	0.754	4667.56	0.273
A5R8	0.775	4276.45	0.277
A5R10	0.793	3926.82	0.274
A7R6	0.725	5226.59	0.276
A7R8	0.748	4780.66	0.269
A7R10	0.769	4398.62	0.259
A9R6	0.701	5688.85	0.267
A9R8	0.726	5199.08	0.254
A9R10	0.748	4784.24	0.244

aligned arc-shaped structure. The design features a circular cross-section with an 11 mm radius and a longitudinal structure length of 50 mm. Key parameters include arc count (A) values of 5, 7, and 9 mm, cell radius (R) values of 6, 8, and 10 mm, and a fixed wall thickness of 1 mm, with an overall structure length of 500 mm. **Fig 1(b)** presents detailed Computer-Aided Design (CAD) of the various gyroid configurations which has different arc account and cell radius. Moreover, **Table 1** provides the detailed geometric characteristics for each gyroid design with relevant structural parameters (viz., porosity, volume, area) that impact thermal absorber performance. The surface area per unit volume enhances fluid-solid interaction, promoting efficient heat transfer, and flow resistance [35]. Porosity (ε) (i.e., the void space fraction) is critical for facilitating fluid flow within the structure, contributing to improved thermal management [36].

The RO-Gyroid structure was fabricated using a DLP printer (*Phrozen Sonic Mini 8K Phrozen Tech Co., Ltd.*). The photopolymer resin comprised HDDA and TMPTA with TPO (*Arkema Sartomer®*) as the UV photoinitiator. Surfactants, dispersants, and anti-settling agents (*BYK Additives & Instruments*) were incorporated, along with 20 wt% milled carbon fibers (*Nippon Polymer Sangyo Co., Ltd.*) to reinforce mechanical and thermal properties. The 20 wt% carbon fiber content was chosen intentionally, drawing from previous studies, which indicated this level achieves an optimal balance for thermal conductivity (ranging from 5 to 10 W/m·K) [37] and mechanical stability, as higher fiber content can lead to brittleness and reduced Young's modulus [28]. **Fig. 2(a)** illustrates the manufacturing process of the RO-Gyroid configurations reinforced with carbon fiber and **Fig. 2(b)** depicts a milled carbon fiber composite printed by DLP, while **Fig. 2(c)** present the surface microstructure of the resulting RO-gyroid taken by scanning electron microscopy (*FESEM, JSM-7900F, JEOL, Ltd., Japan*).

3. Experiment apparatus and test procedure

3.1. Experimental apparatus

The experimental setup, shown in **Fig. 3(a)**, was designed to evaluate flow and heat transfer characteristics of the RO-Gyroid structure designs detailed in **Table 1**. Room temperature air is supplied by a regulated air compressor (*Model TM0210, ASAHI, Japan*) to maintain consistent pressure, with a downstream flow meter (*Alicat Scientific, USA, ± 0.6 %*) monitoring the volumetric flow rate. Two thermocouples (*TECPEL, Taiwan, ± 0.1* ℃) positioned 125 mm downstream and upstream of the heated section records the inlet and outlet temperatures, respectively. The RO-Gyroid is housed within a

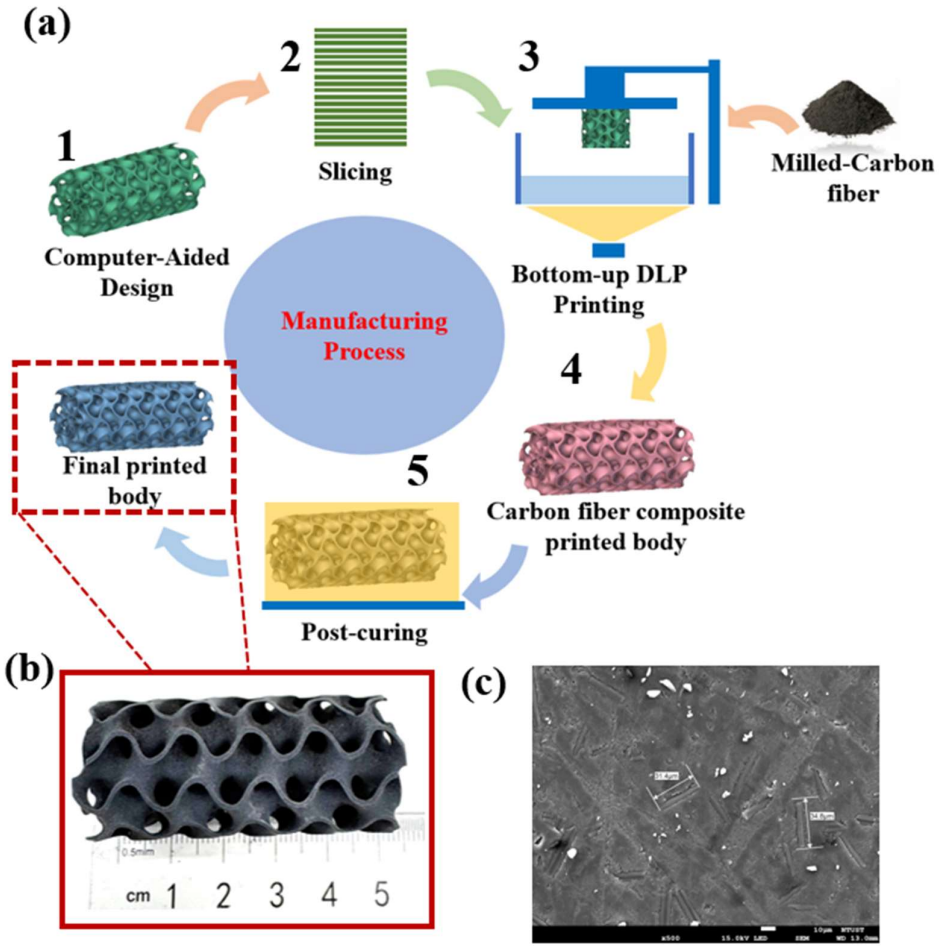

Fig. 2. Fabrication of RO-Gyroid**: (a)** Schematic of the milled carbon fiber RO-Gyroid fabrication process using DLP; **(b)** 20 wt.% milled carbon fiber composites printed by DLP; **(c)** The surface microstructure of the 20 wt.% milled carbon fiber composite.

50 mm cylindrical chamber and is externally heated by an electric band heater (*ARICO Technology Co., Taiwan*) coupled with PID control (*Berm Inc., China*) to ensure controlled temperature rise across the porous structure. A digital manometer (*LINXINO, China, ± 0.29 FSO*) was also used to measure the pressure drop along the flow line. To minimize the heat loss to the environment and ensure uniform heating at 475 K (≈200 ℃), the flow duct was insulated with heat resistant aluminum silicate thermal insulator material. The experiments were conducted using the following procedures with this experimental apparatus:

1. Air is pressured and regulated at room temperature.
2. Flow meter records the volumetric flow rate of the air, with inlet velocities ranging from 0.43 m/s to 1.28 m/s.
3. A thermocouple records the temperature of the gas flow before its interaction with the RO-Gyroid structure.
4. Air flows through the duct and is heated by the heater, enabling convective heat transfer across the RO-Gyroid structure.
5. The digital manometer measures the pressure drop between inlet and outlet of the RQ-gyroid structure.
6. Finally, a secondary thermocouple measures the exit temperature of the gas flow, ensuring the free outflow boundary condition to prevent back-pressure.

3.2 Data processing

The equations for the experimental procedures are detailed in Eqs. (2)-(9) [13,38–40]. Key parameters, such including as the Reynolds number (*Re*), hydraulic diameter (*Dh*), convective heat transfer (*h*), the logarithmic mean temperature difference ΔT_{LMTD}, Nusselt number (*Nu*), friction factor (*f*), and the performance evaluation criteria (*PEC*) for each configuration are determined using these equations.

The Reynolds number represents the ratio of inertial forces to viscous forces in fluid flow, which helps determine whether the flow is laminar (smooth) or turbulent.

$$Re = \frac{\rho v D_h}{\mu} \tag{2}$$

Where ρ represents the fluid density, D_h is the hydraulic diameter, v is the fluid velocity, and μ denotes the fluid viscosity. The hydraulic diameter of the tube D_h is calculated using the following formula (Eq. 3): where A_G is the wetted surface area of the RO-Gyroid structure.

$$D_h = \frac{4\,\varepsilon}{A_G} \tag{3}$$

The heat transfer performance of the RO-Gyroid configurations was evaluated by calculating the convective heat transfer coefficient (*h*) and the Nusselt number (*Nu*). The convective heat transfer coefficient represents the rate at which heat is transferred through convection compared to conduction in the fluid. This coefficient was determined using the corresponding equation.

$$h = \frac{\rho v A_{in} C (T_{out} - T_{in})}{A_h\, \Delta T_{LMTD}} \tag{4}$$

Here, A_{in} refers to the inlet cross-sectional area, *C*

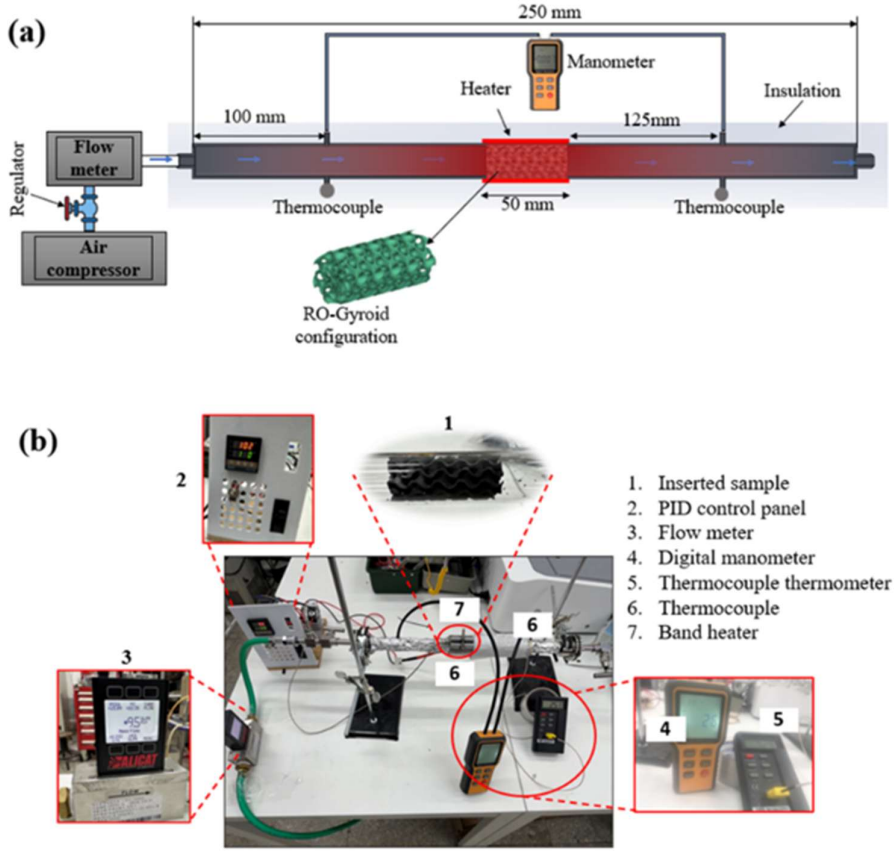

Fig. 3. Description of the experimental setup: **(a)** Schematic representation and **(b)** Representative photograph of the apparatus.

represents the specific heat capacity of air, and T_{in} and T_{out} denote the inlet and outlet fluid temperatures, respectively. The heating surface area is defined by A_h, and the logarithmic mean temperature difference ΔT_{LMTD} is calculated as shown in the following equation.

$$\Delta T_{LMTD} = \frac{(T_{out}-T_{in})}{\ln\left(\frac{T_A-T_{in}}{T_A-T_{out}}\right)} \quad (5)$$

In this context, T_A refers to the temperature of the heating surface. Additionally, The Nusselt number was derived using the following equation.

$$Nu = \frac{h\,D_h}{\lambda} \quad (6)$$

In this equation, λ represents the thermal conductivity of the fluid.

The Darcy friction factor f, a widely used dimensionless, is defined as follows.

$$f = \frac{\Delta P D_h}{2L\rho v^2} \quad (7)$$

Overall thermal performance is evaluated using the performance evaluation criteria (PEC). This criterion is widely used to correlate mass transfer and heat transfer coefficients and is a key indicator of overall heat transfer efficiency [36].

$$PEC = \frac{Nu}{\frac{1}{f^3}} \quad (8)$$

To process the data for estimating the convective heat transfer-based PEC and pressure drop, certain assumptions were made and are summarized as follows:

i. The flow is laminar and steady-state
ii. The flow is incompressible (i.e., constant air density)
iii. No radiative heat transfer (due to the low process temperatures)
iv. Conductive heat transfer is negligible (Biot number ($Bi = \frac{h\,D_h}{k}$) < 0.1), where the thermal conductivity (k) of 20 wt% resin-milled carbon fiber composite is 32 $Wm^{-1}.K^{-1}$ [41]
v. Uniform material properties
vi. Constant heat flux
vii. Negligible heat loss to surroundings owing to insulation layer
viii. No mass transfer and chemical degradation

4. Result and Discussion

4.1. Convective heat transfer

The RO-Gyroid structure enhances heat transfer by promoting a high degree of thermal interaction between the fluid and the structure's surface. **Fig. 4(a)** shows the convective heat transfer coefficients across various RO-Gyroid configurations as a function of *Re* number. The high specific surface area configurations like A9R6 achieved superior heat transfer 32.47 $Wm^{-2}.K^{-1}$, 120.81 $Wm^{-2}.K^{-1}$, 273.84 $Wm^{-2}.K^{-1}$ respectively in each *Re* number. Conversely, the high-porosity but lower surface area design of A5R10 resulted in reduced convective heat transfer coefficient of 8.741$Wm^{-2}.K^{-1}$, 30.787 $Wm^{-2}.K^{-1}$, 84.25 $Wm^{-2}.K^{-1}$, underscoring the importance of the surface area in heat transfer efficiency.

4.2. Friction factor

The friction factor (f) characterizes flow resistance in RO-Gyroid structures, representing energy loss due to fluid friction. **Fig 5(a)** depicts the variation in the friction factor across various design configurations studied and a range of *Re* numbers. The friction factor decreased as the *Re* number increases, which aligns with the typical behavior observed within porous structures [11]. The A9R6 configuration demonstrates significantly higher friction factors at lower *Re* numbers, indicating greater resistance to fluid flow due to their denser structures. This observation is consistent with previous sections, where these configurations exhibited higher pressure drops. As the *Re* number increases, the friction factor for all configurations converges to lower values, with A5R10 showing the least flow resistance due to their higher porosity and lower surface area. At *Re* numbers above 1200, differences in friction factors among configurations become less pronounced, indicating that at inertial forces primarily drive pressure losses, which reduces the impact of geometric design on flow resistance. However, at lower *Re* numbers, the geometry still significantly affects the friction factor.

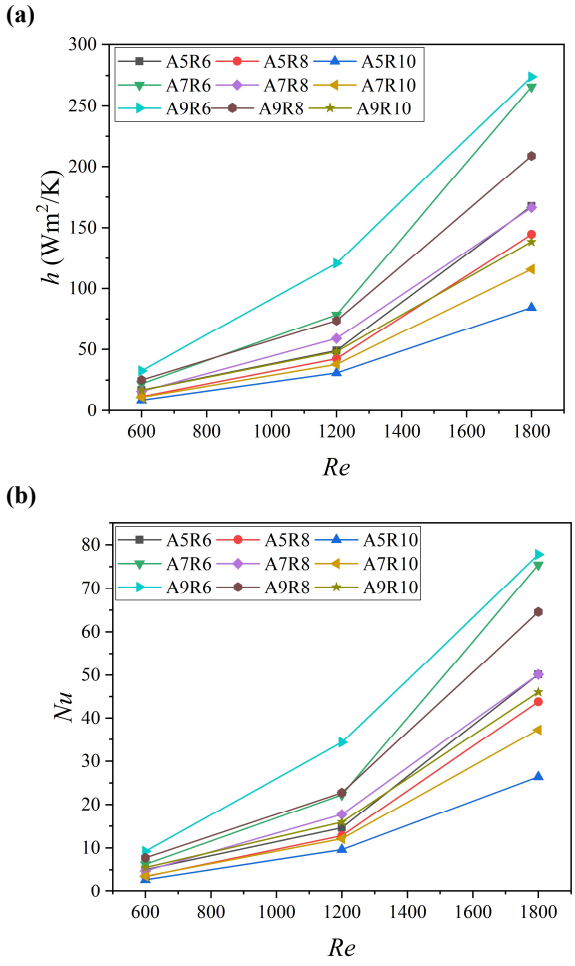

Fig. 4 (a) Convective heat transfer coefficient and **(b)** *Nu* number variation with respect to *Re* number.

4.3. Performance evaluation criteria

The Performance Evaluation Criterion (PEC) is a dimensionless metric that evaluates the thermal-hydraulic performance of RO-Gyroid configurations, balancing heat transfer efficiency with pressure drop for a comprehensive system assessment. **Fig. 5(b)** shows PEC variations with *Re* numbers across configurations, indicating that PEC rises with increasing *Re* numbers. In particular, *Re* >1200, the RO-Gyroid structures improve heat transfer efficiency relative to pressure loss. Among the configurations, A9R6 achieved the highest PEC at *Re* numbers of 600, 1200, and 1800, while A5R10 showed a lower PEC. It is attributed to higher specific surface areas of A9R6 design, which exhibited lower friction factors. As such, the A9R6 configuration demonstrated superior PEC of 5.8 over the other designs due to its higher surface area.

(a)

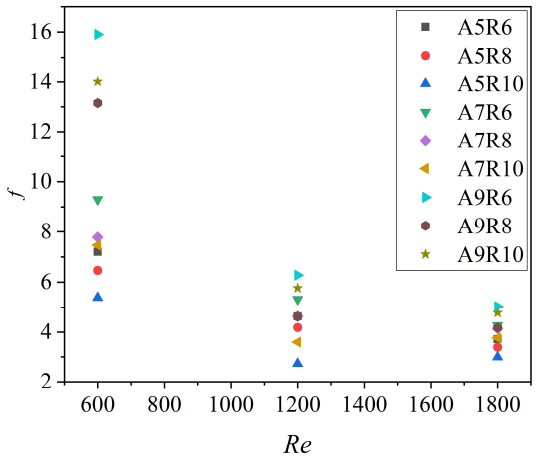

(b)

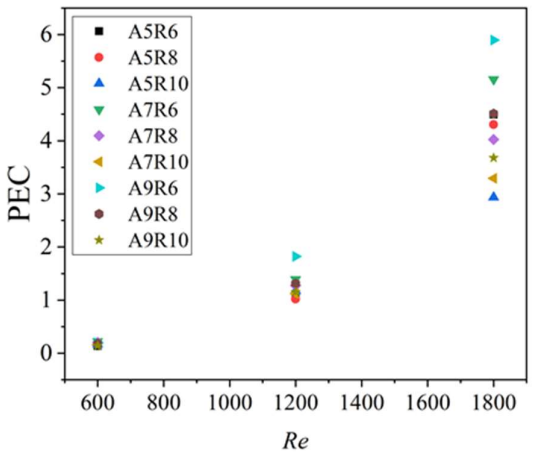

Fig. 5 (a) Frication factor; **(b)** PEC variation with respect to *Re* number.

5. Conclusion

This study successfully fabricated various Radially Oriented Gyroid (RO-Gyroid) configurations via Digital Light Processing (DLP) and systematically assessed their thermal-hydraulic performance for low-temperature thermal absorbers. The key takeaways from the study are:

- Increasing arc count enhances convective heat transfer by 30%, while increasing the cell radius reduces overall heat transfer performance.
- Surface area plays a critical role, with configurations like A9R6 achieving a high heat transfer coefficient of 273.85 W/m²·K due to a favourable surface area-to-volume ratio.
- High-porosity designs, such as A5R10, demonstrated efficient fluid flow with a low-pressure drop of 50 Pa; however, it exhibited lower heat transfer efficiency, underscoring the trade-off between porosity and thermal performance.
- Friction factor analysis revealed that at higher *Re* numbers, inertial forces reduced the influence of structural geometry on flow resistance.
- The A9R6 stands out as the optimal gyroid design configuration, achieving a PEC value of 5.89, which effectively balances heat transfer and pressure loss This makes this design configuration a strong candidate for low-temperature thermal absorber applications.

Future research could expand on this study by using Computational Fluid Dynamics (CFD) simulations and optimization techniques to further enhance thermal and hydraulic performance of the RO-Gyroid configurations. Alongside experimental evaluations, design optimization algorithms -incorporating fiber orientation considerations- could be employed to systematically identify the optimal gyroid configuration for specific performance criteria.

Acknowledgements

Acknowledge that this research is supported by NSTC 112-2222-E-011-003.

Credit authorship contribution statement

Muhtadin Muhtadin: Writing-original draft, Methodology, experimental setup, Conceptualization. **Semih Akin**: Writing-review & editing, Supervision. **Jung Ting-Tsai**: Writing-review & editing, Supervision, Project administration, Funding acquisition, Conceptualization.

References

[1] Ilyas M, Mu Z, Akhtar S, Hassan H, Shahzad K, Aslam B, et al. Renewable energy, economic development, energy consumption and its impact on environmental quality: New evidence from South East Asian countries. Renew Energy 2024;223. https://doi.org/10.1016/j.renene.2024.119961.

[2] Østergaard PA, Duic N, Kalogirou S. Sustainable development using integrated energy systems and solar, biomass, wind, and wave technology. Renew Energy 2024:121359. https://doi.org/10.1016/j.renene.2024.121359.

[3] Ahmadi A, Ehyaei MA, Doustgani A, El Haj Assad M, Hmida A, Jamali DH, et al. Recent residential applications of low-temperature solar collector. J Clean Prod 2021;279. https://doi.org/10.1016/j.jclepro.2020.123549.

[4] Ahmadi A, Ehyaei MA, Doustgani A, Assad MEH, Esmaeilion F, Hmida A, et al. Recent progress in thermal and optical enhancement of low temperature solar collector. Energy Systems 2023;14:1–40. https://doi.org/10.1007/s12667-021-00473-5.

[5] Chen X, Chen Y, Fu L, Zhang Z, Tang M, Feng J, et al. Photovoltaic-driven liquid air energy storage system for combined cooling, heating and power towards zero-energy buildings. Energy Convers Manag 2024;300. https://doi.org/10.1016/j.enconman.2023.117959.

[6] Akbarzadeh S, Valipour MS. Heat transfer enhancement in parabolic trough collectors: A comprehensive review. Renewable and Sustainable Energy Reviews 2018;92:198–218. https://doi.org/10.1016/J.RSER.2018.04.093.

[7] Yılmaz İH, Mwesigye A, Göksu TT. Enhancing the overall thermal performance of a large aperture parabolic trough solar collector using wire coil inserts. Sustainable Energy Technologies and Assessments 2020;39. https://doi.org/10.1016/j.seta.2020.100696.

[8] Hou G, Yadav A, Ali E, Naeem YA, Ahmed FF, Muzammil K, et al. Thermal performance improvement for parabolic trough solar collectors integrated with twisted fin and nanofluid: Modeling and validation. Case Studies in Thermal Engineering 2024;60. https://doi.org/10.1016/j.csite.2024.104763.

[9] Abidi A, El-Shafay AS, Degani M, Guedri K, Mohammad Sajadi S, Sharifpur M. Improving the thermal-hydraulic performance of parabolic solar collectors using absorber tubes equipped with perforated twisted tape containing nanofluid. Sustainable Energy Technologies and Assessments 2022;52. https://doi.org/10.1016/j.seta.2022.102099.

[10] Arshad Ahmed K, Natarajan E. Thermal performance enhancement in a parabolic trough receiver tube with internal toroidal rings: A numerical investigation. Appl Therm Eng 2019;162. https://doi.org/10.1016/j.applthermaleng.2019.114224.

[11] Vasanthip R, Jaya G, Reddyp C. Experimental Investigations On Heat Transfer And Friction Factor Of Hybrid Nanofliud Equiped With Angular Twisted Strip Inserts In A Parabolic Trough Solar Collector Under Turbulent Flow. vol. 8. 2021.

[12] Liu P, Zheng N, Liu Z, Liu W. Thermal-hydraulic performance and entropy generation analysis of a parabolic trough receiver with conical strip inserts. Energy Convers Manag 2019;179:30–45. https://doi.org/10.1016/j.enconman.2018.10.057.

[13] Tang W, Zhou H, Zeng Y, Yan M, Jiang C, Yang P, et al. Analysis on the convective heat transfer process and performance evaluation of Triply Periodic Minimal Surface (TPMS) based on Diamond, Gyroid and Iwp. Int J Heat Mass Transf 2023;201. https://doi.org/10.1016/j.ijheatmasstransfer.2022.123642.

[14] Chen F, Jiang X, Lu C, Wang Y, Wen P, Shen Q. Heat transfer efficiency enhancement of gyroid heat exchanger based on multidimensional gradient structure design. International Communications in Heat and Mass Transfer 2023;149. https://doi.org/10.1016/j.icheatmasstransfer.2023.107127.

[15] Dutkowski K, Kruzel M, Rokosz K. Review of the State-of-the-Art Uses of Minimal Surfaces in Heat Transfer. Energies (Basel) 2022;15. https://doi.org/10.3390/en15217994.

[16] Reynolds BW, Fee CJ, Morison KR, Holland DJ. Characterisation of Heat Transfer within 3D Printed TPMS Heat Exchangers. Int J Heat Mass Transf 2023;212. https://doi.org/10.1016/j.ijheatmasstransfer.2023.124264.

[17] Attarzadeh R, Rovira M, Duwig C. Design analysis of the "Schwartz D" based heat exchanger: A numerical study. Int J Heat Mass Transf 2021;177. https://doi.org/10.1016/j.ijheatmasstransfer.2021.121415.

[18] Attarzadeh R, Attarzadeh-Niaki SH, Duwig C. Multi-objective optimization of TPMS-based heat exchangers for low-temperature waste heat recovery. Appl Therm Eng 2022;212. https://doi.org/10.1016/j.applthermaleng.2022.118448.

[19] Tu J, Qi C, Li K, Tang Z. Numerical analysis of flow and heat characteristic around micro-ribbed tube in heat exchanger system. Powder Technol 2022;395:562–83. https://doi.org/10.1016/j.powtec.2021.10.009.

[20] Choi KH, Cho JR, Shim DS. Effect of heat transfer in substrate on microstructure and tensile behavior of deposits built by directed energy deposition. Journal of Materials Research and Technology 2024;28:3911–31. https://doi.org/10.1016/j.jmrt.2023.12.234.

[21] Pelanconi M, Barbato M, Zavattoni S, Vignoles GL, Ortona A. Thermal design, optimization and additive manufacturing of ceramic regular structures to maximize the radiative heat transfer. Mater Des 2019;163. https://doi.org/10.1016/j.matdes.2018.107539.

[22] Chaudhary R, Fabbri P, Leoni E, Mazzanti F, Akbari R, Antonini C. Additive manufacturing by digital light processing: a review. Progress in Additive Manufacturing 2023;8:331–51. https://doi.org/10.1007/s40964-022-00336-0.

[23] Wu Y, Su H, Li M, Xing H. Digital light processing-based multi-material bioprinting: Processes, applications, and perspectives. J Biomed Mater Res A 2023;111:527–42. https://doi.org/10.1002/jbm.a.37473.

[24] Gibson I, Rosen D, Stucker B. Additive manufacturing technologies: 3D printing, rapid prototyping, and direct digital manufacturing, second edition. Springer New York; 2015. https://doi.org/10.1007/978-1-4939-2113-3.

[25] García-Collado A, Blanco JM, Gupta MK, Dorado-Vicente R. Advances in polymers based Multi-Material Additive-Manufacturing Techniques: State-of-art review on properties and applications. Addit Manuf 2022;50. https://doi.org/10.1016/j.addma.2021.102577.

[26] Oh SH, An CH, Seo B, Kim J, Park CY, Park K. Functional morphology change of TPMS structures for design and additive manufacturing of compact heat exchangers. Addit Manuf 2023;76. https://doi.org/10.1016/j.addma.2023.103778.

[27] Bue D, Skov J, Nørgaard H, Hofstaetter T, Pedersen DB, Nielsen JS, et al. General rights Investigation of digital light processing using fibre-reinforced polymers Investigation of digital light processing using fibre-reinforced polymers. 2024.

[28] Lu C, Deng K, Porter A, Fu K (Kelvin). Top-down digital light processing 3D printing of composite structures using carbon fiber modified UV curable resin. Adv Compos Hybrid Mater 2023;6. https://doi.org/10.1007/s42114-022-00605-0.

[29] Makarian K, Taghvaei M, Tu J, Alvarez NJ, Palmese GR. Design, manufacturing, and elastic analysis of digital light processing 3D printed fiber reinforced sandwich beams with thermosetting polymer matrix. Compos Struct 2023;318. https://doi.org/10.1016/j.compstruct.2023.117108.

[30] Mahmoud D, Tandel SRS, Yakout M, Elbestawi M, Mattiello F, Paradiso S, et al. Enhancement of heat exchanger performance using additive manufacturing of gyroid lattice structures. International Journal of Advanced Manufacturing Technology 2023;126:4021–36. https://doi.org/10.1007/s00170-023-11362-9.

[31] Kwasi-Effah CC, Ibhadode O, Qureshi A. Thermo-hydraulic performance characteristics of novel G-Prime and FRD Triply Periodic Minimal Surface (TPMS) geometries. International Communications in Heat and Mass Transfer 2024;159. https://doi.org/10.1016/j.icheatmasstransfer.2024.108226.

[32] Kelly JP, Finkenauer LR, Roy P, Stolaroff JK, Nguyen DT, Ross MS, et al. Binder jet additive manufacturing of ceramic heat exchangers for concentrating solar power applications with thermal energy storage in molten chlorides. Addit Manuf 2022;56. https://doi.org/10.1016/j.addma.2022.102937.

[33] Szatkiewicz T, Laskowska D, Bałasz B, Mitura K. The Influence of the Structure Parameters on the Mechanical Properties of Cylindrically Mapped Gyroid TPMS Fabricated by Selective Laser Melting with 316L Stainless Steel Powder. Materials 2022;15. https://doi.org/10.3390/ma15124352.

[34] Wang Y, Ren X, Chen Z, Jiang Y, Cao X, Fang S, et al. Numerical and experimental studies on compressive behavior of Gyroid lattice cylindrical shells. Mater Des 2020;186. https://doi.org/10.1016/j.matdes.2019.108340.

[35] Hou Z, Yang C, Wang H, Li H. Heat transfer characteristics and optimization strategies in supercritical fluid heat exchangers with non-uniform thermal boundaries: A systematic review. Int J Heat Fluid Flow 2024;110. https://doi.org/10.1016/j.ijheatfluidflow.2024.109582.

[36] Dube Kerme E, Hajialibabei M, Ziad Saghir M, El-Ketan O. Experimental investigation of porous gyroid structure: Effect of cell size and porosity on performance. Thermal Science and Engineering Progress 2024;53. https://doi.org/10.1016/j.tsep.2024.102728.

[37] Li M, Ali Z, Wei X, Li L, Song G, Hou X, et al. Stress induced carbon fiber orientation for enhanced thermal conductivity of epoxy composites. Compos B Eng 2021;208. https://doi.org/10.1016/j.compositesb.2020.108599.

[38] Barakat A, Sun BB. Controlling TPMS lattice deformation for enhanced convective heat transfer: A comparative study of Diamond and Gyroid structures. International Communications in Heat and Mass Transfer 2024;154. https://doi.org/10.1016/j.icheatmasstransfer.2024.107443.

[39] Sarabhai S, Letov N, Kibsey M, Sanchez F, Zhao YF. Understanding the flow and thermal characteristics of non-stochastic strut-based and surface-based lattice structures. Mater Des 2023;227. https://doi.org/10.1016/j.matdes.2023.111787.

[40] Wang J, Chen K, Zeng M, Ma T, Wang Q, Cheng Z. Investigation on flow and heat transfer in various channels based on triply periodic minimal surfaces (TPMS). Energy Convers Manag 2023;283. https://doi.org/10.1016/j.enconman.2023.116955.

[41] Li M, Ali Z, Wei X, Li L, Song G, Hou X, et al. Stress induced carbon fiber orientation for enhanced thermal conductivity of epoxy composites. Compos B Eng 2021;208. https://doi.org/10.1016/j.compositesb.2020.108599.